Int. J. Heat Mass Transfer. Vol. 23, pp. 1337–1350

0017-9310/80/1001-1337 $02.00/0

NATURAL CONVECTIVE FLOW BETWEEN A BODY AND ITS SPHERICAL ENCLOSURE

RALPH E. POWE,* ROBERT O. WARRINGTON† and JACK A. SCANLAN‡

(*Received* 12 *November* 1979 *and in revised form* 7 *February* 1980)

Abstract—This paper considers in detail the natural convective flow phenomena which occur between a body of relatively arbitrary shape and its spherical enclosure. This is accomplished by combining new experimental flow results with previously available data. New flow visualization results are presented for eccentric spheres and for vertical cylinders inside the spherical enclosure. By considering all the data combined, trends in the behavior of the convective analysis of enclosed body problems than is now possible. Although these results are strictly valid only for a spherical outer body, they give a preliminary indication of expected behavior for other shapes.

NOMENCLATURE

- D, diameter (cylinder diameter for cylindrical inner bodies);
- e, eccentricity measured as distance from center of outer sphere to center of inner body (positive upward);
- g, gravitational acceleration;
- Gr, Grashof number, $g\beta L^3\Delta T/\nu^2$;
- H, overall height of cylindrical inner body;
- L, characteristic dimension for Grashof number, $(D_o - D_i)/2$;
- Pr, Prandtl number, $\nu/\bar{\alpha}$;
- R_L, Rayleigh number, $GrPr$;
- T, temperature;
- ΔT, temperature difference between inner and outer body, $T_i - T_o$;
- α, cylinder aspect ratio, $(H - D_i)/(D_o - D_i)$;
- $\bar{\alpha}$, thermal diffusivity;
- β, thermal expansion coefficient;
- ν, kinematic viscosity.

Subscripts

- i, refers to inner body;
- o, refers to outer body.

INTRODUCTION

FOR MANY years, the problem of natural convection from a body to a surrounding fluid of infinite extent has received a great deal of attention. In recent years, considerable interest has been shown in the problem of natural convection in confined fluids, as is evidenced by the rapidly increasing number of publications in the literature on this subject. This problem is of importance in nuclear reactor technology, electronic instrumentation packaging, aircraft cabin design, the analysis of fluid suspension gyrocompasses, and numerous other practical situations. Accurate prediction of such heat transfer rates, which can now only be roughly approximated, is required in many engineering design problems. Since natural convection flow fields are buoyancy driven due to thermal effects, the thermal fields and hydrodynamic fields are very closely coupled, and a knowledge of the flow field is essential to the complete understanding of the heat transfer phenomena. Also, the unusual stability conditions associated with this problem are of fundamental interest in the fields of heat transfer and fluid mechanics.

From an analytical standpoint the problem of natural convection in enclosed spaces is complicated by the fact that boundary layer approximations and simplifying assumptions regarding pressure gradients normally made in the analysis of simple bodies in an infinite atmosphere are not valid for enclosed spaces. As a result, analytical solutions have been developed only for simple enclosures (defined as containing no enclosed body) and for the simplest enclosed body geometries, horizontal concentric cylinders and concentric spheres. Batchelor [1], Poots [2] and Gill [3] obtained solutions for natural convection within a rectangular cavity with one vertical wall heated and the other cooled. Batchelor expanded the temperature and stream function in power series of the Rayleigh number and evaluated the first few terms in each of these series to generate a solution valid for small Rayleigh numbers. Poots utilized expansions in the form of double series of orthogonal polynomials. Gill analyzed the problem for large Rayleigh numbers and employed a modified Oseen linearization to couple boundary layer and core solutions. A similar solution has been developed by Ostrach [4] for natural convection within a long horizontal cylinder with assymmetric heating, and Weinbaum [5] develops a perturbation solution similar to that of Batchelor for this geometry at small Rayleigh numbers.

Much less work is available regarding enclosed

* Associate Dean, College of Engineering, Mississippi State University, Mississippi State, MS, U.S.A.

† Assistant Professor, Mechanical Engineering Department, Montana State University, Bozeman, MT, U.S.A.

‡ Professor, Mechanical Engineering Department, Montana State University, Bozeman, MT, U.S.A.

body geometries. Perturbation solutions for low Rayleigh numbers have been developed for horizontal concentric cylinders [6–8] and for concentric spheres [9, 10]. Numerical integration of the governing equations for steady laminar flow between horizontal concentric cylinders has been presented by Crawford and Lemlick [11], Abbott [12], and Powe, Carley and Carruth [13], but these solutions are still generally valid only for low Rayleigh numbers since the flow becomes unsteady for large values of the Rayleigh number. Also, computational time is generally excessive. A similar geometry, vertical concentric cylinders, has been investigated numerically by Davis and Thomas [14].

The first experimental studies of natural convection in simple enclosures which began to give an understanding of the basic heat transfer and flow phenomena were those of Eckert and Carlson [15] and Elder [16] for rectangular cavities and that of Brooks and Ostrach [17] for a horizontal cylinder. Three distinct flow and heat transfer regimes were defined as a result of these studies:

(1) a conduction regime for low Rayleigh numbers characterized by linear temperature profiles across the cavity and rotation of the entire fluid mass;
(2) a boundary layer regime for large Rayleigh numbers characterized by thin boundary layers surrounding a large core of almost stagnant, but thermally stratified, fluid;
(3) a transition regime for intermediate Rayleigh numbers.

For larger Rayleigh numbers, secondary flows and unsteady flows were found to occur for many situations.

Experimental investigations of enclosed body geometries have been limited to spherical and cylindrical shapes. For air contained between long horizontal concentric cylinders, flow visualization studies have been conducted by Bishop *et al.* [18, 19], Powe *et al.* [20], and Grigull and Hauf [21]. Heat transfer measurements have been made by Grigull and Hauf [21] and Lis [22]. Liu, Mueller and Landis [23] have extended both flow and heat transfer studies to include other fluids, such as water and silicone oils. The first experimental studies of natural convection in air contained between concentric spheres were conducted by Bishop *et al.* [24, 25], and these have recently been extended to cover a variety of fluids [26, 27]. In addition, heat transfer results have been obtained for slight perturbations from the concentric sphere geometry. Eccentric spheres have been studied by Weber *et al.* [28], while McCoy *et al.* [29] have considered a vertical cylinder within a spherical enclosure.

The purpose of the current paper is to consider in detail the natural convection flow phenomena which occur between a body of relatively arbitrary shape and its spherical enclosure. This will be accomplished by combining new experimental flow results with the previously available data. New flow visualization results will be presented for eccentric spheres and for vertical cylinders inside the spherical enclosure. By considering all the data combined, trends in the behavior of the convective phenomena can be established, and this should enable a much more reliable analysis of enclosed body problems than is now possible. Although these results are strictly valid only for a spherical outer body, they should give a preliminary indication of expected behavior for other shapes.

APPARATUS AND PROCEDURE

The flow visualization apparatus utilized has previously been described in detail by Yin, Powe, Scanlan and Bishop [27], so only the overall characteristics will be given here. Modifications will be discussed in detail, however. The basic apparatus consisted of a glass sphere mounted in a cubical plexiglass enclosure. Various copper inner bodies could be placed inside the sphere in either a concentric or a vertically eccentric position. Two types of inner bodies were used in conjunction with the 24.82 cm I.D. outer (glass) sphere. These included cylinders 11.43 cm in diameter by 16.51 cm in length, 11.43 cm in diameter by 21.59 cm in length, and 17.78 cm in diameter by 22.86 cm in length and spheres having an O.D. of 11.43 cm and 17.78 cm. The cylinders were operated in concentric positions, and the spheres were operated in vertically eccentric locations.

The inner bodies, which were painted flat black to minimize reflections, were supported in the outer sphere by a 1.27 cm diameter stainless steel stem which was insulated on its lateral surface. The inner body surface temperature was kept uniform by a heating tape arrangement. Adhesive backed metallic tapes, 0.051 cm thick and 0.32 cm in width, were spirally affixed to the inner surface of these bodies. As many as eight different tape segments were utilized in each body, and the power input to each of these segments could be individually controlled. To insure that the tapes remained in place, a thin layer of silicone sealant was applied over the entire surface, and the bodies were filled with a loose insulating material before being used. The power input to each of the heater segments could then be adjusted until an isothermal inner body surface was achieved. Surface temperatures were monitored by a number of variously spaced thermocouples.

The outer sphere consisted of two glass hemispheres joined together using a silicone sealant which yielded leak-proof sealing and ease of disassembly for changing the inner body. The surface temperature of this sphere was monitored by six thermocouples attached to the inner surface. An isothermal surface was maintained by a forced air draft through the cubical enclosure and over the outer sphere when air was used as the test fluid and by chilled circulating water when water or either of the silicone oils was under study.

A thin collimated vertical plane of light from two 650 W, air cooled, high intensity quartz–iodine lamps

passed through the vertical axis of the outer sphere. After injection of tracer particles into the gap, this permitted visual and photographic observation of the flow in a plane by viewing at right angles to the collimated light beam. With air as the test fluid, cigar smoke was used to make the flow visible, and the detergent technique developed by Powe *et al.* [30] was used to provide tracer particles in the water.

Since the silicone oils had not previously been used for visualization in a confined space, it was necessary to develop suitable visualization methods for these fluids. Tracer particles were obtained by spraying fluorescent paint over a free surface of the oil. This paint would separate into small particles which would diffuse throughout the fluid. These particles remained in suspension indefinitely and appeared to follow the flow without difficulty.

The procedure used in visualizing the flow patterns was as follows. First, the inner body and the outer body were independently brought to isothermal conditions so as to yield the desired temperature difference. Then, after the flow pattern had stabilized, flow visualization was accomplished, and the flow patterns were recorded with photographs. Throughout this work, all fluid properties are based on the arithmetic mean temperature of the inner body and the outer body, and the characteristic dimension in the Grashof number is taken to be the difference between outer and inner body radii. For concentric spheres, this dimension reduces to the gap width between the two spheres.

FLOW PATTERN RESULTS

Since fluid flow is a part of all convection problems, it has been realized that careful observations of the flow are necessary in order to gain an understanding of measured heat transfer rates and temperature distributions. Thus, heat transfer and temperature field investigations have been accompanied by flow visualization studies. Table 1 indicates the specific geometries and test fluids for which such flow studies have been conducted. These results will be discussed in the following manner. First, for a given fluid, typical flow pattern characteristics will be established, and specific exceptions to these typical characteristics will be noted. Whenever sufficient data are available, categorizations of the patterns into various flow regimes will be presented. Finally, the effect of Prandtl number on the flow patterns for a given geometry will be discussed.

Table 1. Available flow visualization results. (1—data obtained by Bishop *et al.* [24], 2—data obtained by Yin *et al.* [27], 3—data obtained in current investigation)

	Concentric spheres	Eccentric spheres	Cylinder-sphere
Air	1, 2, 3	3	3
Water	2		3
20 cs			3
350 cs	3	3	3

Air

For air as the test fluid, Table 2 indicates geometries for which flow visualization data are available. As with other fluids, for small Rayleigh numbers the flow was found to be steady and laminar, but as the Rayleigh number was increased above some critical value the flow became unsteady. The characteristics of these unsteady patterns were much more dependent on the geometry than were the characteristics of the steady patterns. In many cases secondary flows occurred at the higher Rayleigh numbers, and the onset of turbulence was observed for some geometries.

The basic steady flow pattern observed for low Rayleigh numbers with air as the test fluid has been termed a crescent eddy pattern as a result of its characteristic shape. This pattern, illustrated in Fig. 3 of Bishop *et al.* [25] has been observed for horizontal concentric cylinders [20] as well as for spherical geometries. This pattern was first described by Bishop *et al.* [24] for concentric spheres. It consists basically of thin high speed layers immediately adjacent to the solid surfaces and a large central core of relatively slow moving fluid. Although the velocities in the upflow and downflow regions are much greater than those throughout the remainder of the gap, they are not equal; the upflow velocity is considerably larger than the downflow velocity. This is in agreement with the trend predicted by the analytical solution of Mack and Hardee [9] for low Rayleigh numbers. The fluid in the lower portion of the flow field is relatively stagnant; flow appears to enter this region from the downflow along the outer sphere, and an equal amount of fluid appears to be withdrawn from the lower gap region by the upflow near the inner sphere. This conforms to the prediction of Mack and Hardee [9] that the radial velocity in the upper portion of the flow field will be considerably greater in magnitude than that in the lower portion. Generally, the eddy center is located roughly 60 degrees below the top of the vertical axis (or 30° above the horizontal centerline) and slightly nearer the outer sphere than the inner sphere. The perturbation solution [9] predicts an upward movement of this eddy center with increasing Rayleigh number, as well as a very slight outward movement. From the experimental results, it would appear that the location has become essentially fixed for larger Rayleigh numbers.

The essential characteristics of the crescent eddy pattern were not changed as the shape of the inner body was varied. In cases where the inner and outer bodies were in relatively close proximity in the upper portion of the gap the eddy center was observed to be shifted downward toward the horizontal centerline at lower Rayleigh numbers, as predicted by the perturbation solution.

Table 2. Geometries for available flow visualization results for air (* indicates data from current investigation)

Concentric spheres		Eccentric spheres			Cylinder-sphere		
D_o/D_i	Ref.	D_o/D_i	e/L	Ref.	D_o/D_1	α	Ref.
1.19	[24]	1.40	+0.750	*	1.40	0.722	*
1.37	[24]	1.40	+0.375	*	2.17	0.380	*
1.40	[27]	1.40	−0.375	*			
1.72	[24]	1.40	−0.750	*			
1.78	[27]	2.17	+0.750	*			
2.17	[27]*	2.17	+0.375	*			
2.53	[24]	2.17	−0.375	*			
3.14	[24]	2.17	−0.750	*			

A second steady flow pattern, illustrated in Fig. 5 of Bishop *et al.* [25], was observed for the larger diameter ratios studied. The central low speed portion of the cellular flow pattern became distorted into a kidney shape for moderate Rayleigh numbers. This pattern gives the appearance that fluid is being entrained into the high speed upflow layer in the vicinity of the horizontal axis of the outer sphere. The amount of distortion of the central portion of the flow field was observed to increase with increasing Rayleigh number. Like the crescent eddy pattern, the kidney shaped eddy pattern was completely steady with time. This pattern was first described by Bishop *et al.* [24] for a diameter ratio of 3.14, and Yin *et al.* [27] found that it occurred for diameter ratios of 1.78 and larger. The present investigation has shown that, even for variations in the inner body shape, this pattern still continues to occur for the stated diameter ratio range.

Few variations of these two steady flow patterns have been noted for any of the geometries studied. In cases where the inner and outer body are in very close proximity in the upper portion of the flow field, such as with cylinders of large aspect ratio or spheres with a large positive eccentricity, the fluid apparently cannot penetrate the upper gap region at the smallest Rayleigh numbers studied. This results in an area of stagnant fluid, or of two steady secondary cells, but this region was always filled by the crescent eddy pattern as the Rayleigh number was increased. This pattern is shown in Fig. 4 of Yin *et al.* [27] for concentric spheres with a diameter ratio of 1.40.

Another variation of the basic steady pattern occurred for negative eccentricities with the largest diameter ratio used in the eccentric sphere studies. For small Rayleigh numbers, the crescent eddy pattern did occur, but for moderate Rayleigh numbers, two additional cells were formed in the core region of the pattern. Figure 1 shows this flow pattern. This flow normally existed only for a small range of Rayleigh numbers, the kidney shaped eddy pattern being formed prior to unsteadiness with increasing Rayleigh number.

For all inner body configurations which have been utilized, an unsteady flow pattern occurs when the Rayleigh number exceeds a transition value, and the exact nature of the unsteady flow has been found to be dependent on the geometry. It should be noted that, for Rayleigh numbers only slightly above the transition value, very small deviations from steady flow were observed. In fact, the transition Rayleigh number is defined as the smallest value of the Rayleigh number for which any unsteadiness can be observed in the flow field. As the Rayleigh number is increased above the transition value, however, the unsteadiness becomes increasingly more pronounced.

Basically four different types of unsteady flow have been observed with the spherical outer body. The type of unsteady flow which will occur for a given geometry seems to depend primarily, though not entirely, on the relative spacing between the inner body and the outer body in the upper portion of the flow field. For large spacings, the high speed surface flow layers are essentially unaffected by the unsteadiness, which is concentrated in the interior core region. In contrast, for small spacings strong secondary flows occur, and large portions of the flow pattern are periodically disrupted.

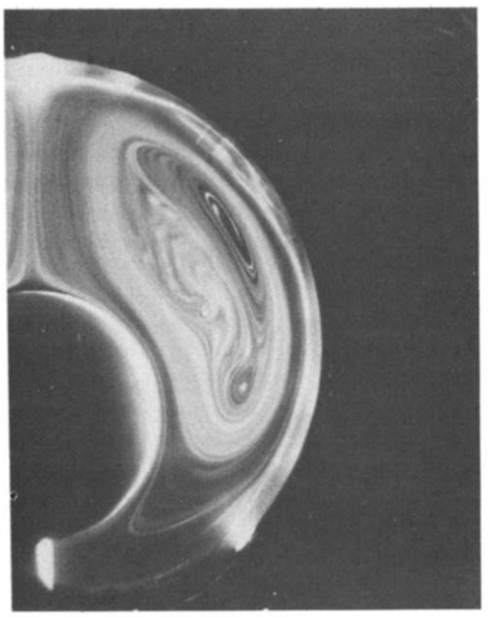

FIG. 1. Steady flow pattern at moderate Rayleigh numbers for air with negative eccentricity.

For concentric spheres with small diameter ratios, Bishop *et al.* [24] observed a 'falling-vortices' pattern, characterized by the formation and shedding of small vortex cells. These vortices formed in counter-rotating pairs in the upper region adjacent to the vertical axis of symmetry. Upon the formation of a second pair of counter-rotating cells, the four cells began to merge into an elongated shape which then appeared to drain into the outer-sphere boundary while at the same time the central eddy rose. This action resulted in a momentary reversion to the single crescent eddy type of flow pattern, which immediately began to break into vortex cells as before. This pattern is shown in Fig. 6 of Bishop *et al.* [25].

For intermediate diameter ratios, a similar, though perhaps more violent, unsteady flow occurs. The high speed flow along the surface of the inner body breaks away from the surface and shoots into the upper portion of the gap resulting in rolling vortices in counter rotation with each other. These cells are associated with sideways oscillations about the vertical, and occasionally the cells are disrupted but are immediately reformed. Following disruption of the rolling vortices, the fluid in the upper region of the gap flows downward via the inner surface of the outer sphere, returning to the lower portion of the annulus with a three dimensional spiral motion. Following this action, the up-flow region adjacent to the inner sphere expands to a relatively large thickness to again throw fluid into the upper region. This pattern is illustrated photographically in Fig. 2.

Unsteadiness in the two remaining types of flow patterns for large Rayleigh numbers appear only in the interior portion of the flow field. For the largest diameter ratios studied the unsteady flow is termed a modified kidney shaped eddy pattern and is shown in Fig. 5 of Yin *et al.* [27]. The unsteadiness above the transition Grashof number is characterized by a

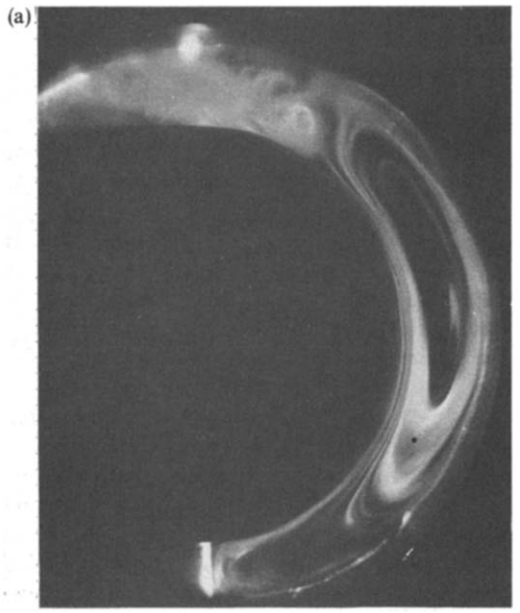

FIG. 2(a).

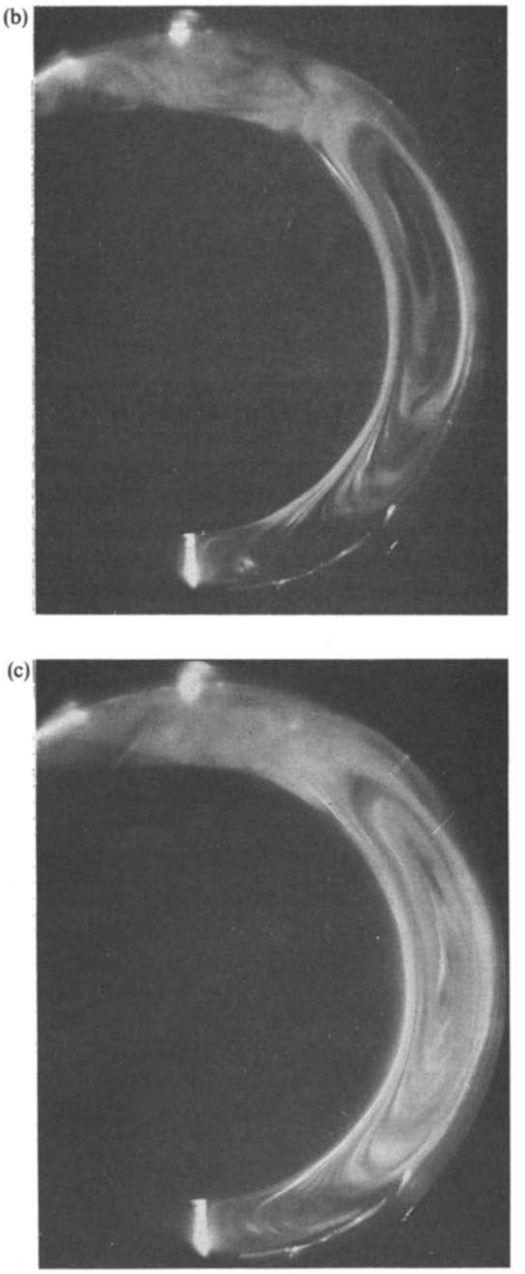

FIG. 2. Three dimensional spiral flow pattern time sequence with air.

continuous shifting of the flow lines in the radial direction from the vicinity of the eddy center toward the inner body. This radially inward shifting flow combines with part of the upward flow and then returns to the lower portion of the low speed central region through the area immediately adjacent to the outer sphere high speed layer.

For slightly smaller diameter ratios, a periodic expansion–contraction motion in the core region characterizes the flow above the transition Rayleigh number. At Rayleigh numbers slightly above the transition value the center of the primary eddy remains visible, but it eventually disappears as the Rayleigh

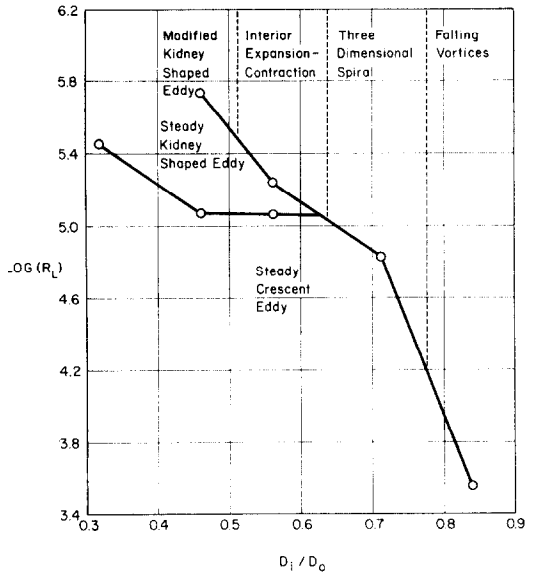

FIG. 3. Flow categorization for air, concentric spheres.

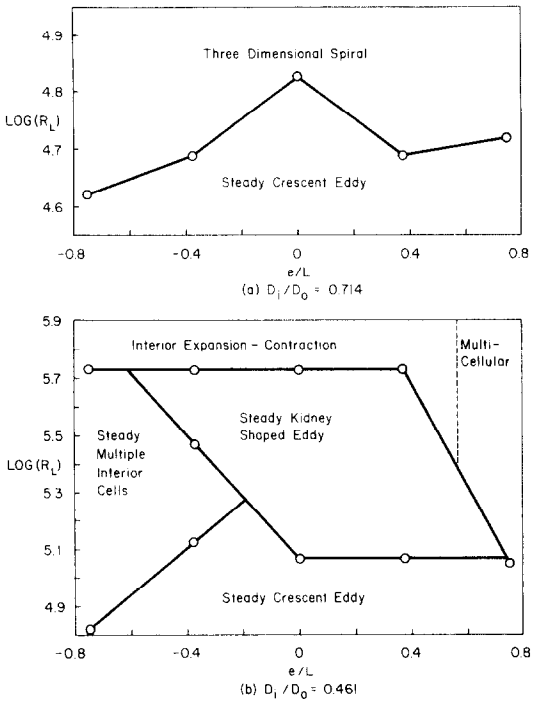

FIG. 4. Flow categorization for air, eccentric spheres.

number is increased. This pattern is shown in Fig. 6 of Yin *et al.* [27].

All of the currently available information concerning flow patterns for concentric spheres is summarized in Fig. 3. For all inverse diameter ratios, the steady crescent eddy pattern occurs at small Rayleigh numbers, while for small inverse diameter ratios, the kidney shaped eddy pattern occurs for moderate Rayleigh numbers. Above the transition Rayleigh number, an unsteady flow always occurs. Certainly the divisions between the various types of unsteady flow are somewhat arbitrary and were simply placed half way between adjacent points. It is interesting to note that when the kidney shaped eddy pattern does appear as a steady pattern, the unsteadiness is likely to be associated with the core region, leaving the wall layers unaffected. On the other hand, for larger inverse diameter ratios where the crescent eddy becomes directly unsteady with increasing Rayleigh number, the unsteadiness is more violent and affects both the core and the wall region. The transition Rayleigh number decreases sharply with increasing inverse diameter ratio, and this is consistent with the observation by Powe *et al.* [20] for horizontal concentric cylinders that the three dimensional type unsteadiness is initiated at much smaller Rayleigh numbers than is the two dimensional unsteadiness.

The critical Rayleigh number for transition from a steady to an unsteady pattern was not found to vary significantly as the inner sphere was moved to an eccentric position except when a change in the type of unsteady flow occurred. In this event a significant change in the transition Rayleigh number was observed. Also, the primary reason for a change in the type of unsteady flow appeared to be reduction of the spacing between inner and outer bodies in the upper portion of the flow field.

Categorization of the flow patterns for air contained between eccentric spheres is presented in Fig. 4. For the larger inverse diameter ratio, 0.714, the unsteady flow is a three dimensional spiral flow in all cases; hence, significant changes in transition Rayleigh number with eccentricity do not occur. However, slight decreases in the transition Rayleigh number are observed as the inner sphere is moved either above or below the center of the outer sphere. This may be explained in the following manner. For negative eccentricities, the length scale associated with the thermal plume rising from the inner sphere is greater than the length scale for concentric spheres. Thus, the plume is more susceptible to disturbances, and a decreased transition Rayleigh number results. On the other hand, for positive eccentricities the high speed flow layer along the inner sphere has more difficulty penetrating the upper gap region due to the decreasing spacing of the bodies here. This causes separation of the flow layer from the inner body to occur at a somewhat lower Rayleigh number than for concentric spheres. Hence, a decrease in the transition Rayleigh number is again noted.

For the smaller inverse diameter ratio shown in Fig. 4, 0.461, the Rayleigh number for transition to an unsteady pattern is completely unaffected by eccentricity, except for the largest eccentricity studied. As in the concentric sphere case, the unsteady flow normally affected only the interior core of the flow field, leaving the high speed layers undisturbed. This unsteadiness consisted of a periodic expansion–contraction motion as described previously. Due to the close proximity of the two bodies along the upward vertical axis, the flow

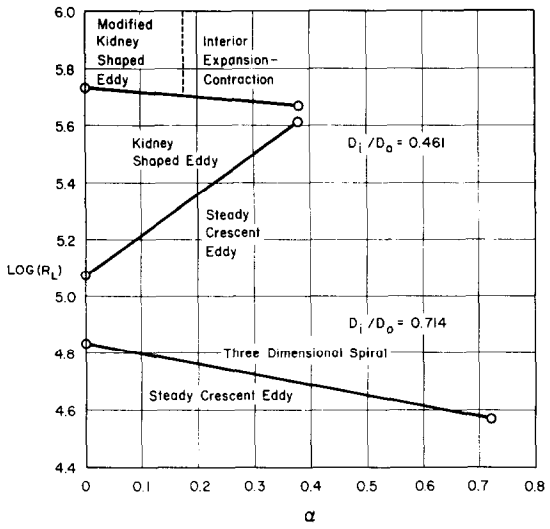

FIG. 5. Flow categorization for air, cylindrical inner body.

does not penetrate the upper gap region for the largest positive eccentricity studied. This results in the three-dimensional spiral type of unsteady flow, and as observed previously, this is initiated at a much smaller Rayleigh number than other types of unsteady flow.

Figure 5 illustrates the various flow regimes observed for inner bodies consisting of vertical cylinders with hemispherical end caps. Concentric sphere data are included as they represent the limiting case of a cylinder of zero height. For the larger inverse diameter ratio the crescent eddy pattern persisted as the steady pattern as the aspect ratio increased. Since the inverse diameter ratio is rather large, the three dimensional spiral flow exists as the unsteady flow for the concentric spheres, and no change in the type of unsteadiness is observed with increasing aspect ratio. A slight decrease in transition Rayleigh number is noted, however, since the high speed layer along the inner body has more difffculty penetrating the upper gap region. For the smaller inverse diameter ratio, increasing the length of the cylindrical section causes some changes in both steady and unsteady patterns. For increasing aspect ratio, the steady kidney-shaped eddy pattern exists over a smaller Rayleigh number range, and it appears that the only steady pattern would be the crescent eddy for aspect ratios larger than about 0.4. The reason for this behavior is perhaps simply that distortion of the central core cannot occur in the presence of the long vertical surfaces. This also leads to a change in the type of unsteady flow with increasing aspect ratio. For concentric spheres, the unsteadiness appears as a modified kidney shaped eddy, but as the kidney shaped eddy disappears below the transition Rayleigh number, the unsteadiness changes to the interior expansion–contraction type. Both of these unsteady flows are associated only with the core region, however, so only s slight decrease in transition Rayleigh number is observed as the aspect ratio increases.

Water

For water as the test fluid, Table 3 indicates geometries for which flow visualization data are available. The basic steady flow pattern obtained for low Rayleigh numbers may be described in terms of three distinct regions. First, in the immediate vicinity of each body a thin high-speed primary flow region is observed. The fluid in this area moves upward along the inner body and downward along the outer sphere with a relatively high speed compared to that in other portions of the gap. As with air, this motion results in a dividing line, or chimney, along the upward vertical axis. Secondly, an interior, low-speed flow region is observed in the upper portion of the annulus. Here there are two secondary flows circulating in the same direction as the primary flow. One of them is attached to the inner body producing a weak return flow to the near vicinity of the inner body. The other appears at the extreme top of the gap adjacent to the chimney, and, evidently, a weak shear layer must occur between these two cells. Finally, the major part of the gap consists of a central stagnant region in which the flow can be detected only by photographs using a relatively long time exposure. This pattern is illustrated in Fig. 8 of Yin *et al.* [27].

Exceptions to the foregoing basic steady pattern for concentric spheres were observed only for the two smallest diameter ratios employed. For the diameter ratio of 1.40 the steady pattern could still be described in terms of the same three regions. However, the locations of the interior secondary cells were tangentially shifted away from the chimney to some extent. This left a region of interior low-speed secondary flow occupying most of the upper portion of the annulus. For the diameter ratio of 1.09, the flow was unsteady throughout the range of obtainable Grashof numbers.

For the cylinder-sphere geometry, the basic steady flow pattern was observed for the larger diameter ratio with an aspect ratio of 0.380. For the aspect ratio of 0.759, the close spacing of the two bodies in the upper portion of the flow field prevented the formation of the secondary cellular flows. Instead, the entire flow pattern more closely resembled the crescent eddy pattern, as illustrated by the sketch in Fig. 6. For the diameter ratio of 1.40 and aspect ratio of 0.722 the flow took on the crescent eddy appearance completely.

Table 3. Geometries for available flow visualization results for water (* indicates data from current investigation)

Concentric spheres		Cylinder-sphere		
D_o/D_i	Ref.	D_o/D_i	α	Ref.
1.09	[27]	1.40	0.722	*
1.40	[27]	2.17	0.380	*
1.78	[27]	2.17	0.759	*
2.17	[27]			

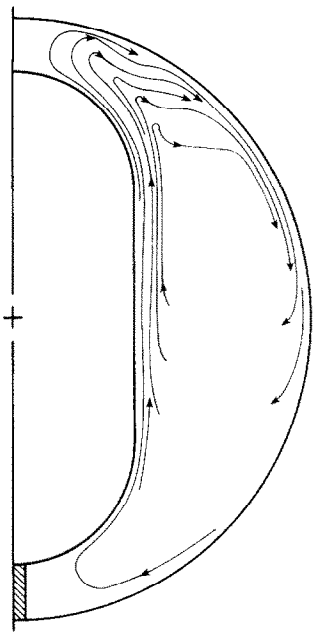

FIG. 6. Sketch of steady flow pattern for water with cylindrical inner body.

The unsteady flows observed with water for Rayleigh numbers above the transition value generally affected only the upper portion of the flow field, and for the two largest diameter ratios with concentric spheres did not affect the wall layers. For the diameter ratio of 2.17, the upper secondary cell is no longer stationary in position when the Rayleigh number is increased above 2.9×10^7. Instead, this cell is alternately formed and then submerged into the relatively stagnant region of the upper interior portion of the annulus, thereby causing a somewhat random motion to occur. Simultaneously, fluid is also discharged from this region along the inner surface of the outer sphere with a rolling vortex motion. This flow phenomenon is repeated with an indefinite period, although the frequency appears to increase with Rayleigh number. This flow is shown in Fig. 9 of Yin *et al.* [27].

For a diameter ratio of 1.78 the steady flow pattern exists undisturbed until a Rayleigh number of 1.0×10^7 is reached. At this point, the weak shear region between the secondary cells expands and becomes a weak tertiary cell, and the upper secondary cell grows in size and changes in shape. On the other hand, the lower secondary cell is reduced in size, and most of the flow in this region returns to the outer sphere high speed layer instead of to the inner sphere layer, as was the case with the steady flow pattern. In addition, a considerable amount of random motion is observed in the interior low speed secondary flow region. This type of unsteady flow is illustrated in Fig. 10 of Yin *et al.* [27].

For the two smallest diameter ratios considered with concentric spheres, a type of falling vortices flow pattern, similar to that obtained in air, occurs for large Rayleigh numbers. This flow pattern is shown in Fig. 11 of Yin *et al.* [27]. When the transition Rayleigh number is exceeded, the flow in the upper portion of the gap randomly alternates between two-dimensional vortex motion and a three dimensional spiral motion. Fluid is continually supplied to this region by flow separated from the upward primary flow along the inner sphere. It was observed that a continuous withdrawal of fluid from this upper region occurs through the portion nearest the outer sphere, and this withdrawn fluid combines with the primary flow to return to the lower portion of the annulus. Only a very slight sideways oscillation occurs in the upper regions, and, occasionally, the continuous withdrawal of fluid from the upper portion of the gap is enhanced by a slug of fluid generated in this vicinity. There is no definite period of occurrence for this phenomenom, however.

For all cylindrical inner bodies, the unsteadiness observed above the transition Rayleigh number was of the three dimensional spiral type, similar to that observed for concentric spheres with a diameter ratio of 1.40. Increasing the cylinder height generally caused this unsteadiness to appear at a smaller Rayleigh number.

The currently available information concerning flow patterns in water contained between concentric spheres is summarized in Fig. 7. The general shape of the transition Rayleigh number curve is not considerably different from that shown for air in Fig. 3. A simple type of steady flow is observed for all inverse diameter ratios, while a number of different types of unsteady flow are observed. For the smaller inverse diameter ratios, the unsteadiness is associated with the

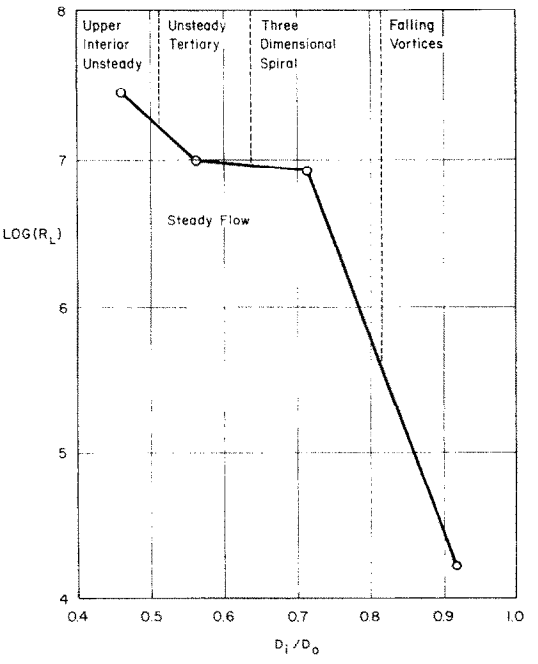

FIG. 7. Flow categorization for water, concentric spheres.

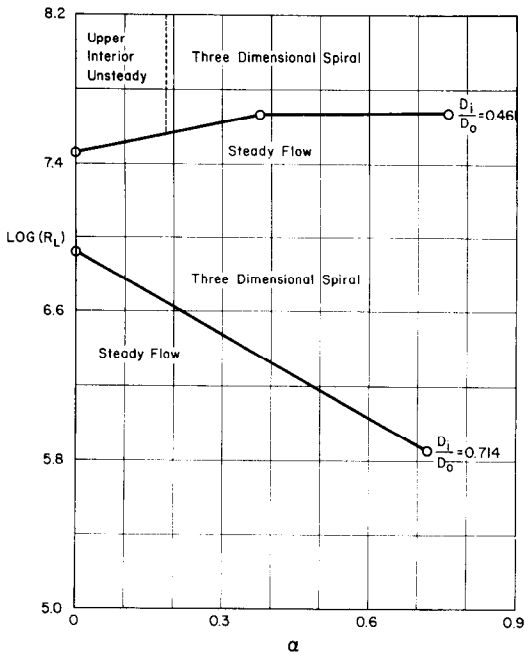

FIG. 8. Flow categorization for water, cylindrical inner body.

upper interior portion of the flow field, while for the larger inverse diameter ratio, the unsteadiness is more violent and affects both the core and the wall region. The transition Rayleigh number decreases very sharply with increasing inverse diameter ratio.

Categorization of the flow patterns in water with the cylindrical inner body is shown in Fig. 8. For the larger inverse diameter ratio, the transition Rayleigh number decreases sharply with increasing aspect ratio. This is due to the increased tendency toward flow separation at the upper junction of cylinder and hemisphere as the cylinder height is increased. For the smaller inverse diameter ratio, the transition Rayleigh number increases slightly as the aspect ratio increases. This is a trend which has not been observed previously. However, it is noted that there is a change in the type of unsteady flow pattern which occurs as the aspect ratio is increased, and this may certainly affect the delay in onset of unsteadiness.

20 cS *fluid*

Table 4 indicates geometries for which flow visualization data are available for the 20 cS fluid. For this particular fluid, only the cylindrical inner body was employed, and ony two of these bodies were tested. Both the steady and the unsteady flows observed for these two bodies were significantly different. For the larger diameter ratio, 2.17, the flow at low Rayleigh numbers appeared to be a combination of the kidney shaped eddy pattern and the basic steady pattern observed in water. Very distinct high speed flow layers were observed adjacent to the solid boundaries, and a plume appeared above the cylinder. The fluid exhibited a tendency to turn downward, prior to striking the enclosing sphere, however, and this resulted in an appearance similar to the steady flow in water in the upper portion of the gap. Although the fluid in the core appeared almost stagnant to the naked eye, very long time exposures of photographic film indicated a kidney shaped eddy in the core region. This steady flow pattern is shown in Fig. 9.

Table 4. Geometries for available flow visualization results for 20 cS fluid (* indicates data from current investigation)

Cylinder-sphere		
D_o/D_i	α	Ref.
1.40	0.722	*
2.17	0.380	*

As would perhaps be anticipated, the unsteadiness with the diameter ratio of 2.17 appeared first in the upper portion of the flow field. The streamlines closed to form a secondary vortex in this area, and this vortex would periodically be dissipated. For the highest Rayleigh numbers considered, numerous small secondary cells appeared immediately adjacent to the high speed flow up the cylinder surface.

For the smaller diameter ratio, 1.40, the steady flow pattern consisted of the usual high speed surface flow layers, but the core region was occupied by numerous secondary cells. This pattern is shown for the lowest Rayleigh number obtained in Fig. 10. As the Rayleigh number was increased, these secondary cells decreased in size while increasing in number and covering a larger portion of the gap. Finally, the flow in the upper gap region became unsteady, and a three dimensional spiral type unsteadiness appeared. However, this unsteadiness did not affect the flow in the central and

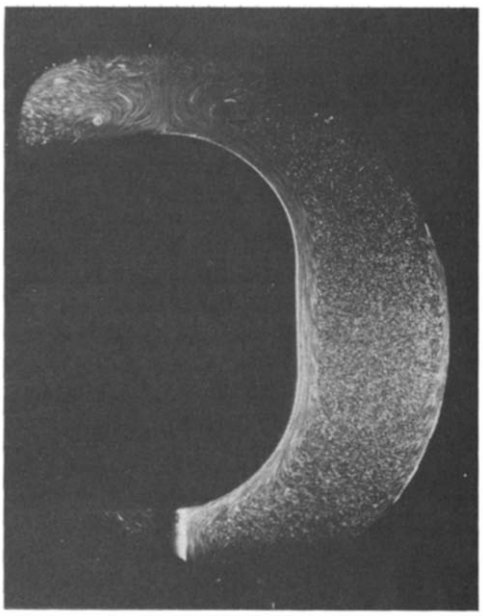

FIG. 9. Steady flow for 20 cS silicone fluid with large diameter ratio.

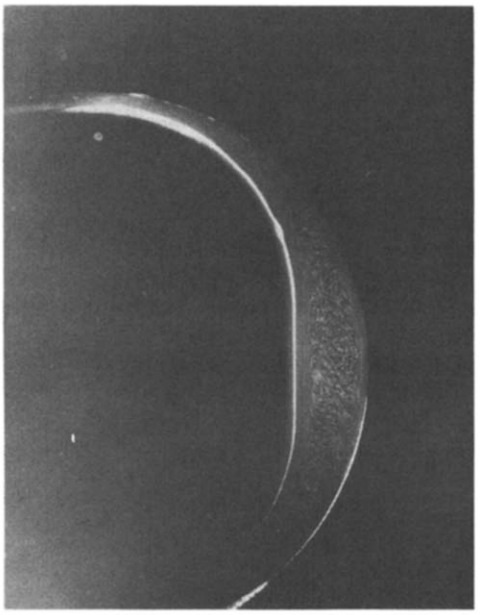

FIG. 10. Steady flow for 20 cS silicone fluid with small diameter ratio.

major portion of the flow field. For these larger Rayleigh numbers, the secondary cells appeared to become divided into vortex pairs, one occurring adjacent to the inner body and the other adjacent to the outer body. This flow pattern is illustrated in Fig. 11 for the largest Rayleigh number obtained.

The available data for the 20 cS silicone fluid are shown in Fig. 12. There are not enough data available to establish trends with aspect ratio. However, the transition Rayleigh number for the larger inverse

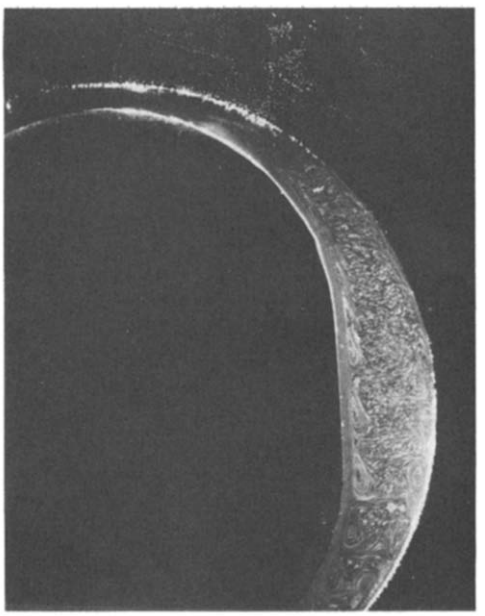

FIG. 11. Unsteady flow for 20 cS silicone fluid with small diameter ratio.

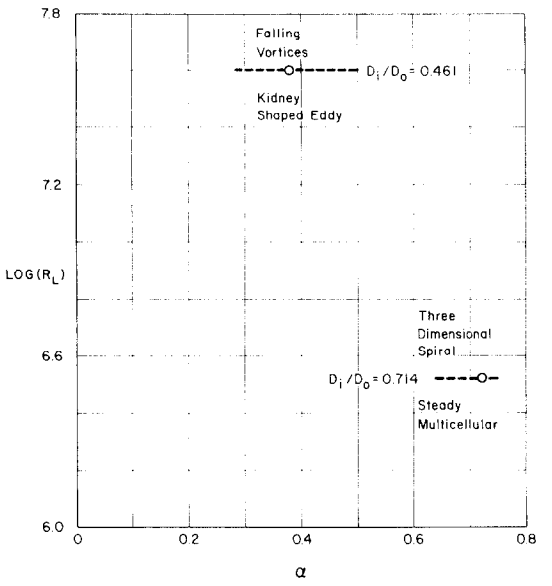

FIG. 12. Flow categorization for 20 cS silicone fluid, cylindrical inner body.

diameter ratio is considerably smaller than that for the smaller inverse diameter ratio. This is consistent with previous trends where the three dimensional spiral type unsteadiness has been observed to be initiated at smaller Rayleigh numbers than other types of unsteady flow.

350 cS *fluid*

Table 5 indicates geometries for which flow visualization data are available for the 350 cS fluid. Somewhat surprisingly, the steady flow pattern observed for low Rayleigh numbers is similar to the crescent eddy type as described for air as the test fluid. The significance difference is that absolutely no motion could be detected in the core region of the flow field, even using photographs with long time exposures. This pattern is illustrated in Fig. 13.

There were two exceptions to the occurrence of this crescent eddy like flow at small Rayleigh numbers. In cases where the two bodies were in close proximity in the upper portion of the gap (small diameter ratio with large positive eccentricity, cylindrical inner body with small diameter ratio and large aspect ratio), the flow could not penetrate this region, thereby resulting in the early inception of unsteady flow. In fact, in some cases, steady flow was not observed for any Rayleigh number used. The second exception occurred for the cylindrical inner body having a large diameter ratio (2.17) and a large aspect ratio (0.759). As shown in Fig. 14, the difference appeared in the upper portion of the flow field where the fluid adjacent to the inner body appeared to drop after leaving the high speed flow layer instead of migrating directly to the outer body high speed flow.

Basically two different types of unsteady flow were observed for this fluid—a three dimensional spiral

Table 5. Geometries for available flow visualization results for 350 cS fluid (* indicates data from current investigation)

Concentric spheres		Eccentric spheres			Cylinder-sphere		
D_o/D_i	Ref.	D_o/D_i	e/L	Ref.	D_o/D_i	α	Ref.
1.40	*	1.40	+0.750	*	1.40	0.722	*
		1.40	−0.375	*	2.17	0.380	*
		1.40	−0.750	*	2.17	0.759	*
		2.17	+0.750	*			
		2.17	+0.375	*			
		2.17	−0.375	*			
		2.17	−0.750	*			

flow (Fig. 15) and unsteady interior secondary flow (Fig. 16). In general, the unsteadiness appeared in the interior core of the flow field for relatively large gap spacings measured at 90° from the upward vertical axis. As in previous cases the high speed flow layers were not affected by this unsteadiness.

Categorization of the flow patterns in 350 cS silicone fluid contained between eccentric spheres is shown in Fig. 17. While the steady crescent eddy pattern is common to all configurations, the type of unsteady flow is seen to be a function of inverse diameter ratio rather than eccentricity. For the larger inverse diameter ratio, where the three dimensional spiral flow occurs, departure from the concentric position is seen to cause a tendency toward unsteady flow. However, for the smaller diameter ratio, where the unsteadiness appears in the core flow, an increase in eccentricity generally leads to a reduction in the transition Rayleigh number. This is true until the inner sphere is placed very near the outer, which appears to have a stabilizing effect.

A summary of results for a cylindrical inner body with 350 cS silicone fluid is shown in Fig. 18. For the larger inverse diameter ratio, the three dimensional spiral flow again appears as the unsteady pattern, and the transition Rayleigh number decreases significantly as the aspect ratio is increased due to an increased tendency toward separation by the surface flow layer on the inner body. For the smaller inverse diameter ratio, the appearance of unsteady secondary cells for an intermediate aspect ratio range leads to a higher transition Rayleigh number than for either small or large aspect ratios where the three dimensional spiral flow again occurs. Although a crescent eddy appears as the steady flow for small Rayleigh members at all aspect ratios, the intermediate aspect ratio range also yields steady interior secondary cells prior to this flow's becoming unsteady.

CONCLUSION

A study of natural convection between a body and its spherical enclosure is presented for fluids with Prandtl numbers ranging from 0.7 to about 4000. The basic steady pattern observed has been termed a crescent eddy flow, and appeared for low Rayleigh numbers for small and large Prandtl numbers. For

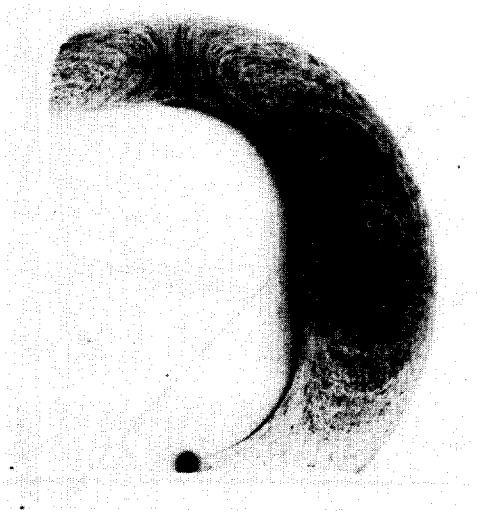

FIG. 13. Steady flow pattern for low Rayleigh numbers with 350 cS silicone fluid.

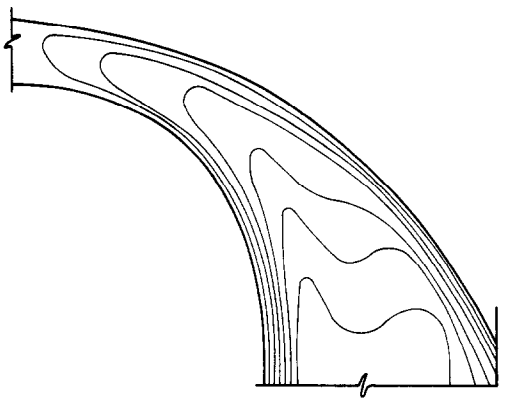

FIG. 14. Flow pattern for low Rayleigh numbers with 350 cS silicone fluid for cylindrical inner body with large diameter ratio and large aspect ratio.

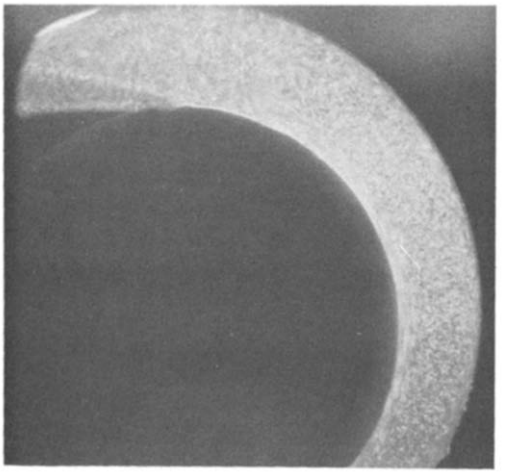

FIG. 15. Three dimensional spiral flow for 350 cS silicone fluid.

intermediate Prandtl number fluids (primarily water) a completely different type of steady pattern occurred, and its onset was generally delayed to a relatively large Rayleigh number, as illustrated in Fig. 19. Many different types of unsteady flow appeared, and the type of unsteady flow was found to be strongly dependent on geometry as well as Prandtl number.

The work reported in this paper should be useful in determining the type of flow to be expected in a variety of situations. It should also prove useful for validation of proposed analytical or numerical techniques.

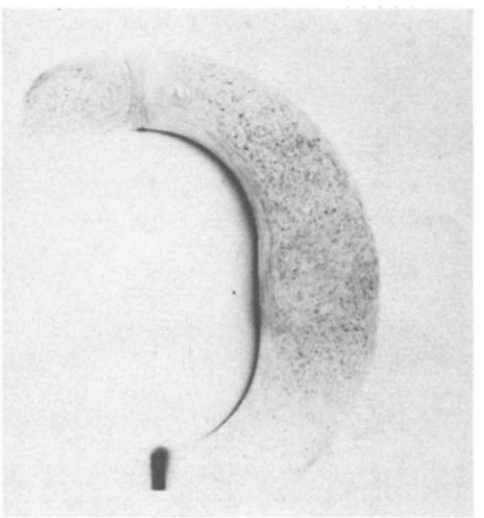

FIG. 16. Unsteady interior secondary flow for 350 cS silicone fluid.

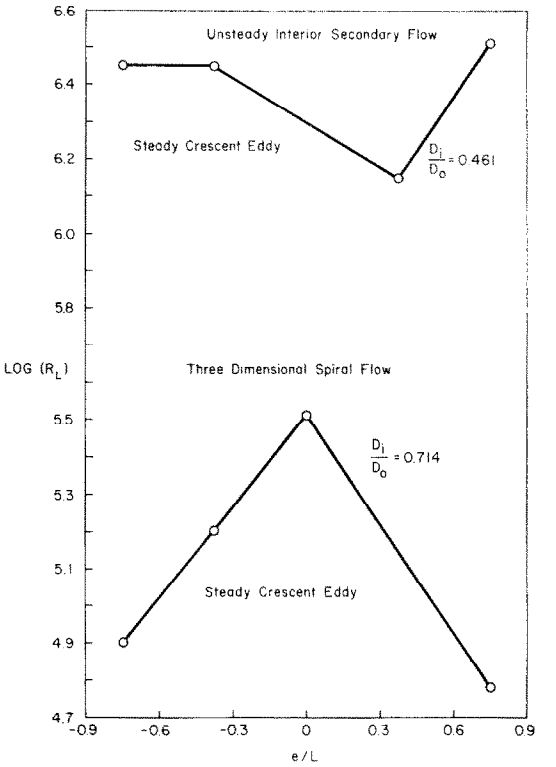

FIG. 17. Flow categorization for 350 cS silicone fluid, eccentric spheres.

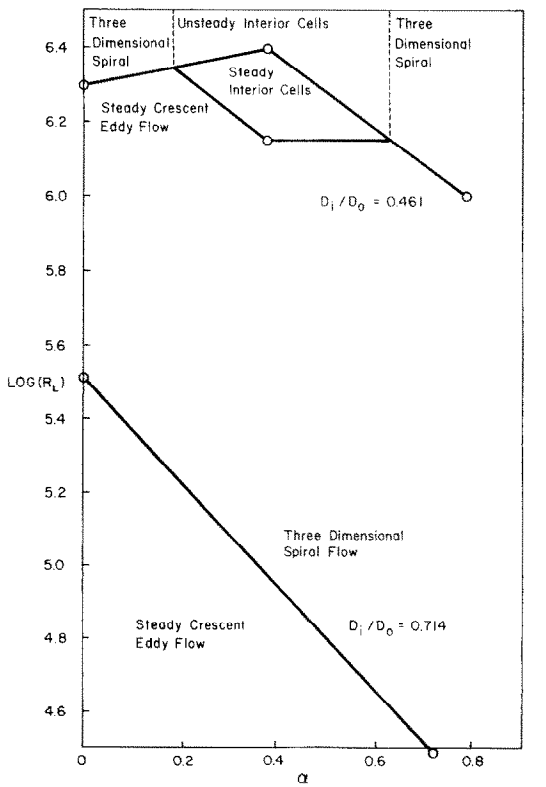

FIG. 18. Flow categorization for 350 cS silicone fluid, cylindrical inner body.

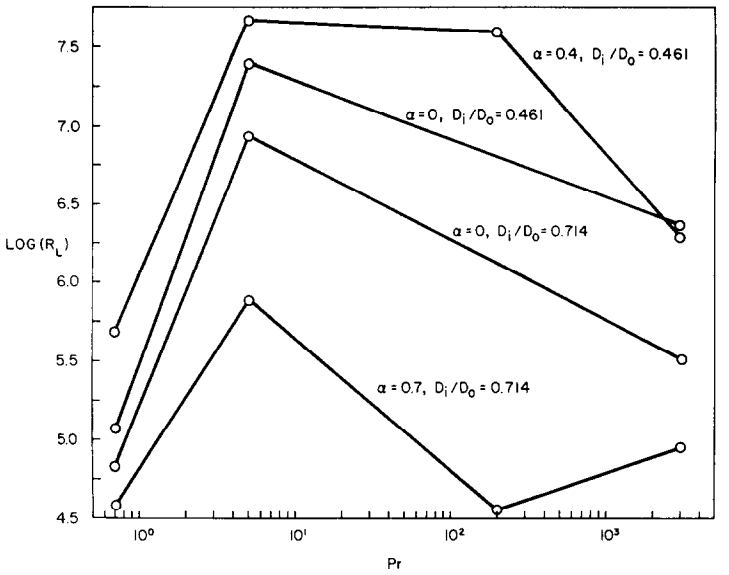

FIG. 19. Effect of Prandtl numbers on transition Rayleigh numbers for selected geometries.

REFERENCES

1. G. K. Batchelor, Heat transfer by free convection across a closed cavity between vertical boundaries at different temperatures, *Q. Appl. Math.* **12**, 3, 209–233 (1954).
2. G. Poots, Heat transfer by laminar free convection in enclosed plane gas layers, *Q. Jl Mech. Appl. Math.* **11**, 3, 257–273 (1958).
3. A. E. Gill, The boundary layer regime for convection in a rectangular cavity, *J. Fluid Mech.* **26**, 3, 515–536 (1966).
4. S. Ostrach, Natural convection in enclosures, *Adv. Heat Transf.* **8**, 161–227 (1972).
5. S. Weinbaum, Natural convection in a horizontal circular cylinder, *J. Fluid Mech.* **18**, 3, 409–437 (1964).
6. L. R. Mack and E. H. Bishop, Natural convection between horizontal concentric cylinders for low Rayleigh numbers, *Q. Jl Mech. Appl. Math.* **21**, 2, 223–241 (1968).
7. Z. Rotem, Conjugate free convection from horizontal conducting circular cylinders, *Int. J. Heat and Mass Transfer* **15**, 1679–1693 (1972).
8. P. F. Hodnett, Natural convection between horizontal heated concentric circular cylinders, *J. Appl. Math. Phys.* **24**, 507–516 (1973).
9. L. R. Mack and H. C. Hardee, Natural convection between concentric spheres at low Rayleigh numbers, *Int. J. Heat Mass Transfer* **11**, 387–396 (1968).
10. F. E. Fendell, Laminar natural convection about an isothermally heated sphere at small Grashof number, *J. Fluid Mech.* **34**, 1, 163–176 (1968).
11. L. Crawford and R. Lemlich, Natural convection in horizontal concentric cylindrical annuli, *I/EC Fundamentals* **1**, 4, 260–264 (1962).
12. M. R. Abbott, A numerical method for solving the equations of natural convection in a narrow concentric cylindrical annulus with a horizontal axis, *Q. Jl Mech. Appl. Math.* **17**, 4, 471–481 (1964).
13. R. E. Powe, C. T. Carley and S. L. Carruth, A numerical solution for natural convection in cylindrical annuli, *J. Heat Transfer* **92**, 210–220 (1971).
14. G. de Vahl Davis and R. W. Thomas, Natural convection between concentric vertical cylinders, *High Speed Computing in Fluid Dynamics, The Physics of Fluids Supplement* **II**, 198–207 (1969).
15. E. R. G. Eckert and W. O. Carlson, Natural convection in an air layer enclosed between two vertical plates with different temperatures, *Int. J. Heat Mass Transfer* **2**, 106–120 (1961).
16. J. W. Elder, Laminar free convection in a vertical slot, *J. Fluid Mech.* **23**, 1, 77–98 (1965).
17. I. H. Brooks and S. Ostrach, An experimental investigation of natural convection in a horizontal cylinder, *J. Fluid Mech.* **44**, 3, 545–561 (1970).
18. E. H. Bishop and C. T. Carley, Photographic studies of natural convection between concentric cylinders, *Proc. 1966 Heat Transfer and Fluid Mechanics Institute*. Stanford University Press, 63–78 (1966).
19. E. H. Bishop, C. T. Carley and R. E. Powe, Natural convective oscillatory flow in cylindrical annuli, *Int. J. Heat Mass Transfer* **11**, 1741–1752 (1968).
20. R. E. Powe, C. T. Carley and E. H. Bishop, Free convective flow patterns in cylindrical annuli, *J. Heat Transfer* **91**, 3, 310–314 (1969).
21. U. Grigull and W. Hauf, Natural convection in horizontal cylindrical annuli, *Proc. Third Int. Heat Transfer Conf.*, AIChE **2**, 182–195 (1966).
22. J. Lis, Experimental investigation of natural convection heat transfer in simple and obstructed horizontal annuli, *Proc. Third Int. Heat Transfer Conf.*, AIChE **2**, 196–204 (1966).
23. C. Y. Liu, Mueller W. K. and F. Landis, Natural convection heat transfer in long horizontal cylindrical annuli, *Int. Dev. Heat Transfer* Part V, 976–984.
24. E. H. Bishop, R. S. Kolflat, L. R. Mack and J. A. Scanlan, Convective heat transfer between concentric spheres, *Proc. 1964 Heat Transfer and Fluid Mechanics Institute*, 69–80. Stanford University Press (1964).
25. E. H. Bishop, L. R. Mack and J. A. Scanlan, Heat transfer by natural convection between concentric spheres, *Int. J. Heat Mass Transfer* **9**, 649–662 (1966).
26. J. A. Scanlan, E. H. Bishop and R. E. Powe, Natural convection heat transfer between concentric spheres, *Int. J. Heat Mass Transfer* **13**, 1857–1872 (1970).
27. S. H. Yin, R. E. Powe, J. A. Scanlan and E. H. Bishop, Natural convection flow patterns in spherical annuli, *Int.*

J. Heat Mass Transfer **16**, 1785–1795 (1973).
28. N. Weber, R. E. Powe, E. H. Bishop and J. A. Scanlan, Heat transfer by natural convection between vertically eccentric spheres, *J. Heat Transfer* **95**, 1, 47–52 (1973).
29. C. T. McCoy, R. E. Powe, E. H. Bishop, N. Weber and J. A. Scanlan, Free convection between a vertical cylinder and a spherical enclosure, *Proc. Fifth Int. Heat Transfer Conf.*, Tokyo (1974).
30. R. E. Powe, S. H. Yin, J. A. Scanlan and E. H. Bishop, A technique for visualization of the very flow motion of water in enclosed spaces, *J. Heat Transfer* **95**, 3, 408–409 (1973).

CONVECTION NATURELLE ENTRE UN CORPS ET SON ENCEINTE SPHERIQUE

Résumé—On considère en détail la convection naturelle entre un corps de forme arbitraire et une enceinte sphérique. Pour cela on combine de nouveaux résultats expérimentaux avec des données déjà existantes. On présente de nouveaux résultats de visualisation pour des sphères excentriques et pour des cylindres verticaux dans l'enceinte sphérique. En considérant toutes les données, des tendances dans le comportement des phénomènes convectifs sont dégagées et ceci montrerait qu'une analyse mieux établie des corps dans une enceinte est possible. Bien que ces résultats sont strictement valables seulement pour une enceinte sphérique, ils donnent une indication sur les comportements dans le cas d'eautres formes.

FREIE KONVEKTIONSSTRÖMUNG ZWISCHEN EINEM KÖRPER UND SEINER KUGELFÖRMIGEN UMHÜLLUNG

Zusammenfassung—Diese Arbeit behandelt ausführlich die Strömungserscheinungen bei freier Konvektion zwischen einem Körper von relativ zufälliger Form und seiner kugelförmigen Umhüllung. Dabei werden neue Ergebnisse experimenteller Strömungsuntersuchungen mit bereits bekannten Daten kombiniert. Neue Ergebnisse der Strömungssichtbarmachung werden für exzentrische Kugeln und für vertikale Zylinder innerhalb einer kugelförmigen Umhüllung angegeben. Durch gemeinsames Berücksichtigen aller Daten werden Trends im Verhalten der Konvektionserscheinungen festgestellt, wodurch eine viel zuverlässigere Behandlung von Problemen eingeschlossener Körper ermöglicht wird als bisher. Obwohl diese Ergebnisse nur für einen kugelförmigen äußeren Körper streng gültig sind, geben sie doch vorab einen Hinweis auf das zu erwartende Verhalten bei anderen Formen.

ЕСТЕСТВЕННАЯ КОНВЕКЦИЯ МЕЖДУ ТЕЛОМ И СФЕРИЧЕСКОЙ ОБОЛОЧКОЙ

Аннотация — Проведено детальное исследование естественной конвекции между телом, имеющим достаточно произвольную форму, и сферической оболочкой. Полученные экспериментальные результаты сопоставлены с ранее имеющимися данными. Представлены новые результаты по визуализации течения между эксцентрическими сферами и по обтеканию вертикальных цилиндров, заключенных в сферическую оболочку. На основании рассмотрения всех имеющихся данных установлен характер конвективного движения, что позволит впредь проводить намного более надежный анализ свободноконвективных процессов для внутренних задач. Несмотря на то, что полученные результаты являются строго справедливыми только для тел, находящихся в сферических оболочках, они позволяют определить примерный характер процессов для тел других конфигураций.